Materials Research Proceedings 28 (2023) 807-816 https://doi.org/10.21741/9781644902479-88

Experimental identification of uncoupled ductile damage models and application in flow forming of IN718

VURAL Hande[1,a], ERDOGAN Can[1,b], KARAKAŞ Aptullah[2,c], FENERCIOGLU Tevfik Ozan[2,d] and YALÇINKAYA Tuncay[1,e *]

[1]Department of Aerospace Engineering, Middle East Technical University, 06800 Ankara, Turkey

[2]Repkon Machine and Tool Industry and Trade Inc., 34980 Şile, Istanbul, Turkey

[a]vural.hande@metu.edu.tr, [b]cane@metu.edu.tr, [c]aptullah.karakas@repkon.com.tr, [d]ozan.fenercioglu@repkon.com.tr, [e]yalcinka@metu.edu.tr

Keywords: Ductile Fracture, Fracture Locus, Flow Forming Process

Abstract. The aim of this study is to calibrate the parameters of the Johnson-Cook (JC) and modified Mohr-Coulomb (MMC) ductile failure models for Inconel 718 and predict the formability limit in the flow forming process using the aforementioned uncoupled damage models. Uniaxial tensile tests are performed on four different specimen geometries to cover a variety of stress states. A hybrid methodology combining finite element simulations and experimental findings is used to calibrate the JC and MMC damage models. The models are implemented in the finite element solver Abaqus using a user-defined subroutine. Results show that the calibrated models agree well with the experimental data in all tensile tests. In shear dominant loads, the MMC model is found to be more capable of showing accurate crack propagation. In flow forming simulations, a significant difference is observed between the JC and MMC models in the prediction of damage. Lode parameter-dependent damage models, such as the MMC, are found to be more suitable for the prediction forming limits in the flow forming process.

Introduction

Flow forming, or spinning, is an incremental metal forming process used to produce axisymmetric parts and it has been widely adopted in the automotive and defense industries (see e.g. [1]). The thickness of a tubular preform material is incrementally reduced by utilizing one or more rotating rollers. It has several benefits such as low scrap material, low cost due to simple tool processing, smooth surface quality, and high geometrical accuracy. The preform thickness can be reduced by up to 80 % throughout the process. Such high deformations under complex forces potentially lead to surface defects or complete rupture. As in many forming applications, it is crucial to identify the regions that are more susceptible to crack initiation or defects and to estimate the formability limits in flow forming.

In computational structural analysis, ductile fracture models have been widely adapted to describe the ductile failure of metallic materials. According to their relationship with constitutive equations, damage models employed in finite element (FE) simulations can be separated into coupled and uncoupled models. Coupled models in which the damage parameters and constitutive equations are coupled, and the stress is influenced by the damage evolution (e.g. [2-4]). Uncoupled models exclude the effect of damage evolution from constitutive relations. They are often referred to through a failure criterion, which consists of plastic strain, strain rate, stress state, and temperature (e. g. [5,6]). Uncoupled models are more common in engineering applications because of their simplicity in implementation and parameter calibration, despite coupled models providing more realistic failure predictions. It has been discussed that a ductile failure criterion depends only on stress triaxiality (T) could be insufficient for shear dominant ductile failures (see [7]). To

overcome this problem, Lode angle parameter ($\bar{\theta}$), which is connected to the third deviatoric stress invariant, has been considered in more recent models (e.g. [8,9]).

In the literature, many attempts have been made to predict forming limits using damage models for incremental metal-forming processes (e.g. [10,11,12,13]). The MMC model is used in one of the authors' earlier studies for flow forming analyses to analyze forming limits and the influence of process parameters in failure. In [14], the MMC model for 6016-T6 aluminum alloy is adopted from the literature to examine the effect of the thickness reduction ratio and the involvement of different roller arrangements on the damage. The strain rate and temperature dependencies for the 4340-steel alloy were included in the plasticity and MMC models in [15], and the implications of process variables including feed rate, roller speed, and offset of the rollers on damage are studied.

The aim of this study is first to calibrate the damage model parameters for Inconel 718 (IN718) through a hybrid experimental-numerical approach. Tensile tests are carried out on four specimen geometries to cover various stress states. The DIC (digital image correlation) technique is used to extract accurate displacement-force values from the experiments. For this material, the plasticity model is constructed using experimental data and FE simulations. The MMC and JC damage models are adopted to model ductile damage. A good correlation between the FE results and the experimental data is achieved with the calibrated models. Then, the failure prediction capabilities of the calibrated damage models are investigated with the simulation of the flow forming process.

Methods

Materials and Tensile Tests.

Tensile tests are performed for IN718 alloy under quasi-static conditions. IN718 is nickel-based precipitation hardenable superalloy where gamma double prime (γ”) precipitations are nucleated after the aging treatment to have improved mechanical properties. IN718 has good fatigue and creep strength with high corrosion resistance, and it has been widely used in the hot sections of gas turbines engines such as turbine discs and blades. The chemical composition of the alloy is given in Table 1. For this material, 4 different specimens representing different stress-state conditions are manufactured. The geometries of the specimens are shown in Fig. 1. Specimens are named as smooth tension (ST), notch tension (NT10), plane-strain tension (PST) and in-plane shear (ISS). Specimens are prepared with a thickness of 3 mm. They are spray-painted in white and then patterned in black dots for displacement and strain measurements with the digital image correlation (DIC) method. MTS 100kN Tension-Torsion Fatigue/Static test machine and a high-speed camera are used to obtain the force and displacement data. Displacement-controlled tests are carried out with a strain rate of 1 mm/min. NCORR open-source 2D DIC software is used to process the images captured by the high-speed camera. Force data is obtained from the test machine while the displacements are extracted from the DIC analysis using a virtual extensometer at the center of the specimens spanning vertically with a gauge length of 40, 50, 8.1, and 28 mm for ST, NT10, PST and ISS specimens, respectively.

Table 1: Chemical composition of IN718 [wt.%].

Element	Ni	Nb	Mo	Ti	Al	Cr	Cu	Si	Fe	Mn	C
Content	54.35	4.96	2.77	0.95	0.56	18.59	0.04	0.32	16.68	0.28	0.5

Plasticity and Damage Models.

The constitutive behavior is governed by the classic J2 plasticity with isotropic hardening. The extended voce rule is used to define the hardening law, as

$$\sigma = \sigma_y + q_1\left(1-c_1 e^{-b_1 \bar{\varepsilon}_p}\right) + q_2\left(1-c_2 e^{-b_2 \bar{\varepsilon}_p}\right) \quad (1)$$

where σ_y is the yield stress of IN718 and $\bar{\varepsilon}_p$ is the equivalent plastic strain. q_i, c_i and b_i are material-specific constants.

Two different damage models are chosen to evaluate their applicability to flow forming simulation. The first of these models is the JC model, which is only stress triaxiality and equivalent plastic strain dependent. Due to its simplicity, it has been frequently used in many applications in the literature. In this study, the JC model is utilized independently of strain rate and temperature, as

$$\varepsilon_f(T) = \widehat{D}_1 + \widehat{D}_2 \exp(-\widehat{D}_3 T) \quad (2)$$

where, T is the stress triaxiality and ε_f is the plastic strain value at failure. $\widehat{D}_1$, $\widehat{D}_2$ and $\widehat{D}_3$ are calibration parameters for the JC model. The second model is the MMC model defined as

$$\varepsilon_f(T, \bar{\theta}) = \left\{ \begin{array}{l} \frac{A}{\widehat{C}_2}\left[\widehat{C}_3 + \frac{\sqrt{3}}{2-\sqrt{3}}\left(\widehat{C}_4 - \widehat{C}_3\right)\left(\sec\left(\frac{\bar{\theta}\pi}{6}\right) - 1\right)\right] \\ x\left[\sqrt{\frac{1+\widehat{C}_1^2}{3}} + \cos\left(\frac{\bar{\theta}\pi}{6}\right) + \widehat{C}_1\left(T + \frac{1}{3}\sin\left(\frac{\bar{\theta}\pi}{6}\right)\right)\right] \end{array} \right\}^{-\frac{1}{n}} \quad (3)$$

where, T is the stress triaxiality, $\bar{\theta}$ is the Lode angle parameter and ε_f is the plastic strain value at failure. A, n, $\widehat{C}_1$, $\widehat{C}_2$, $\widehat{C}_3$ and $\widehat{C}_4$ are calibration parameters for MMC model. Stress triaxiality and Lode angle parameter are formalized as

$$T = \frac{\sigma_m}{\sigma_{eq}} \text{ and } \bar{\theta} = 1 - \frac{6\theta}{\pi} = 1 - \cos^{-1}\left(\frac{J_3}{2\,\sigma_{eq}{}^3}\right) \quad (4)$$

where the mean stress is $\sigma_m = \frac{tr(\sigma)}{3} = \frac{\sigma_{11} + \sigma_{22} + \sigma_{33}}{3}$, σ_{eq} is the von-Mises equivalent stress and J_3 is defined as the third deviatoric stress invariants.

The damage accumulation rule is expressed with the following integral

$$D = \int_0^{\varepsilon_f} \frac{d\bar{\varepsilon}_p}{\varepsilon_f} \quad (5)$$

Initially, the material is assumed to be undamaged, D = 0, and when D reaches 1 and is interpreted as the material is completely failed.

FE Modelling.

Displacement controlled explicit FE simulations are conducted to calibrate and verify the plasticity and damage model parameters. The MMC model is implemented as a user-defined field subroutine (VUSDFLD) while the inbuilt JC damage model in Abaqus is used. The geometries and mesh of 4 different specimens are shown in Fig. 1. One-fourth of geometries are simulated for

ST, NT and PST utilizing the symmetry planes to reduce the computational cost. For the ISS, analysis is taken with the full model. 8-node linear brick elements (C3D8R) with reduced integration are used and element deletion is utilized to represent material failure. To have boundary conditions consistent with experiments, the parts held and pulled in the machine are modeled as rigid bodies while the section where DIC analysis is conducted is modeled as a deformable body.

Calibrated and validated damage models are then applied to the finite element model of the backward flow forming (FF) process using the dynamic explicit solver of Abaqus. The FE model and mesh are shown in Fig. 2. This model consists of a preform, a mandrel, and 3 rollers rotating and moving in the axial direction. The process is called the backward FF process because the material flows in the direction opposite to the axial movement of the rollers. Mandrel and rollers are modeled as rigid bodies while the preform tube is a deformable body. The rollers are placed around the mandrel with 120 degrees between them with a certain axial offset. This ensures that the thickness of the material is incrementally reduced and a thickness reduction ratio of 40% in total is applied. Both tangential and normal contact are featured in the model with a 0.05 friction coefficient for tangential contact. The preform tube is meshed using hexahedral elements with reduced integration (C3D8R) and enhanced hourglass control is used to prevent mesh distortion. There are 168000 elements in total, with 7 elements in the thickness direction.

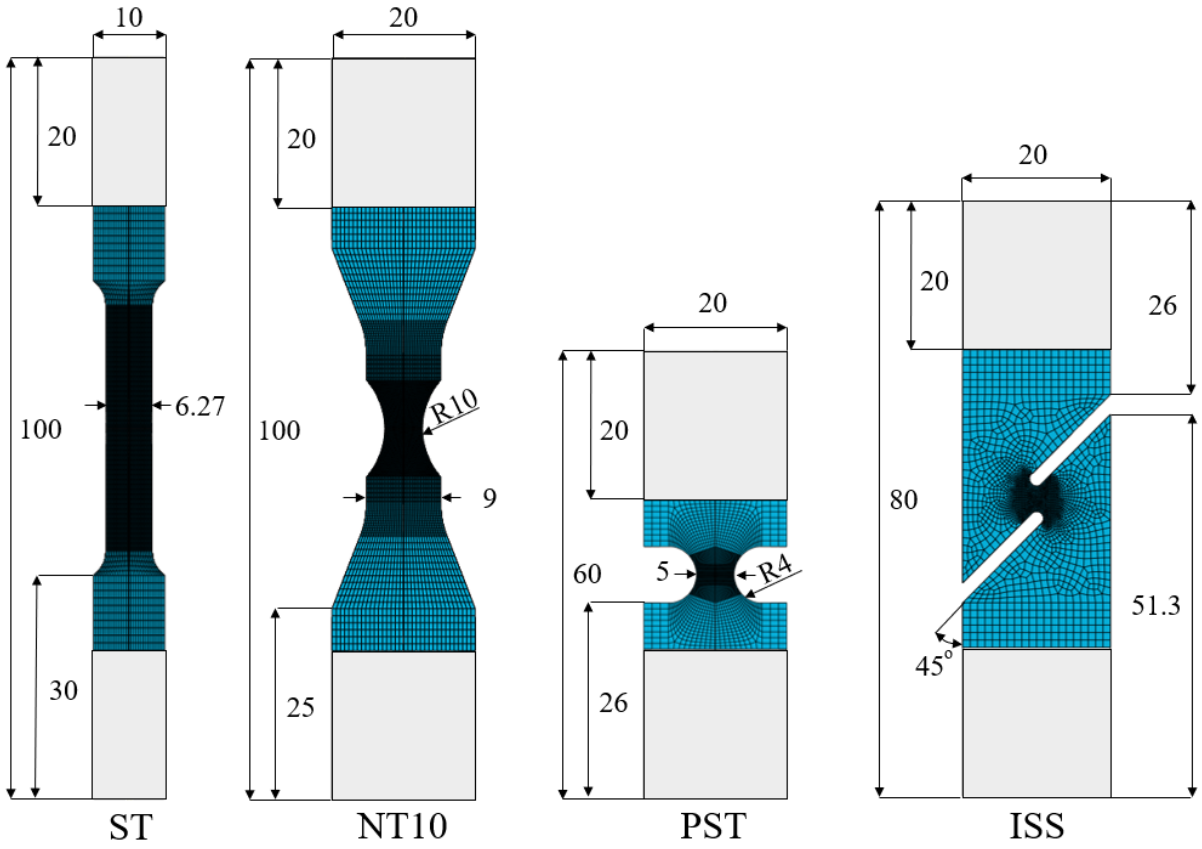

Fig. 1. Dimensions and finite element models of specimens.

Results and Discussion

Plasticity Model Calibration.

Since an uncoupled modeling approach is used in the current work, hardening parameters can be calibrated with the experimental data independently of the damage parameters. Using the force-displacement data obtained from the experiments, the true stress-strains curves are obtained using up to necking from the ST specimen. The hardening law parameters are then fitted using the MATLAB curve-fitting tool. The yield stress and material constants of the hardening laws are shown in Table 2. Density, Young's modulus and Poisson's ratio are taken as 8.22 g/cm^3, 200 GPa and 0.294, respectively.

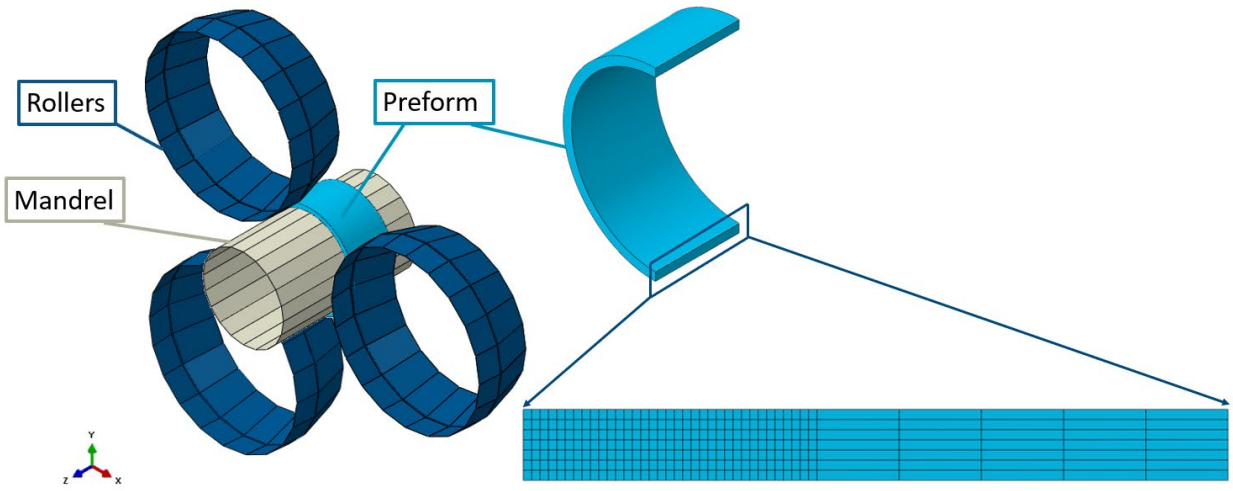

Fig. 2. Finite element model of flow forming process.

Table 2. Calibrated parameters of the hardening law.

σ_y [MPa]	q_1 [MPa]	c_1	b_1	q_2 [MPa]	c_2	b_2
789	499.6	0.1731	106.7	499.6	1.761	4.351

Damage Model calibration.

The MMC damage model parameters are calibrated using a hybrid experimental and numerical approach which has been applied and verified for a wide range of materials and experiments in the literature. In this approach, plastic strain averaged stress triaxiality and Lode angle parameter data are extracted from the FE simulations of the specimens up to the experimentally observed failure point. The place where sudden decreases in force-displacement curves is taken as the fracture initiation and the equivalent plastic strain value at this point is selected as failure strain. The failure strain, averaged T and $\bar{\theta}$ values are taken from the critical elements which have the highest equivalent plastic strain. In ST, NT10 and PST specimens, the critical elements are in the center of the specimens, while the critical points of the ISS are in the middle of the curved region in the gauge section. The failure strain, averaged T and $\bar{\theta}$ values are given in Table 3.

Materials Research Proceedings 28 (2023) 807-816 https://doi.org/10.21741/9781644902479-88

Table 3. Fracture strain, averaged T and $\bar{\theta}$ for all specimens.

Specimen	T_{ave}	$\bar{\theta}_{ave}$	ε_f
ST	0.4040	0.9614	0.6512
NT	0.4849	0.7650	0.5245
PST	0.5494	0.5882	0.4564
ISS	0.1205	0.1546	0.5069

Then, the calibration of the MMC and JC model parameters is simply done using the MATLAB curve fitting tool. Since there are 3 calibration parameters in the JC criterion, using ST, NT10, and PST specimens is sufficient for calibration. For the data given in Table 3, 5 calibration parameters are identified while $\hat{C}_4$ is taken as 1 for the MMC model. Firstly, $\hat{C}_3$ is assumed to be 1 and the other 4 parameters are fitted to the damage criterion. Then, $\hat{C}_3$ is included in the parameter fitting by keeping A as constant. The calibrated damage parameters are given in Table 4.

Table 4. Calibrated parameters of the MMC and JC damage models for IN718.

	$\hat{D}_1$	$\hat{D}_2$	$\hat{D}_3$			
JC	0.04	1.798	2.679			
	A [MPa]	n	$\hat{C}_1$	$\hat{C}_2$	$\hat{C}_3$	$\hat{C}_4$
MMC	1946	2.216	10.39	14420	4.517	1

Ductile Failure Simulations.

The results obtained from FE simulations with the calibrated damage models for 4 different specimens are shown in Fig. 3. Note that experiments are repeated 3 times for each geometry to check variation between specimens. Experimental results are shown with black dashed lines, while the orange and blue solid lines represent JC and MMC simulations, respectively. Due to the changes in manufacturing and micromechanical inhomogeneities, slight variations in failure strain are observed between tests. In the smooth tension test, the variation is found to be higher than normal. Nevertheless, the failure strain value is calibrated based on the average of multiple tests for each specimen geometry. It is clear that the models are able to capture the experimental force-displacement relation for all specimens. In ST, NT10 and PST simulations, JC and MMC models yield almost exactly the same response. However, for ISS specimen, although the failure points predictions are similar, the subsequent failure response is vastly different for the JC model.

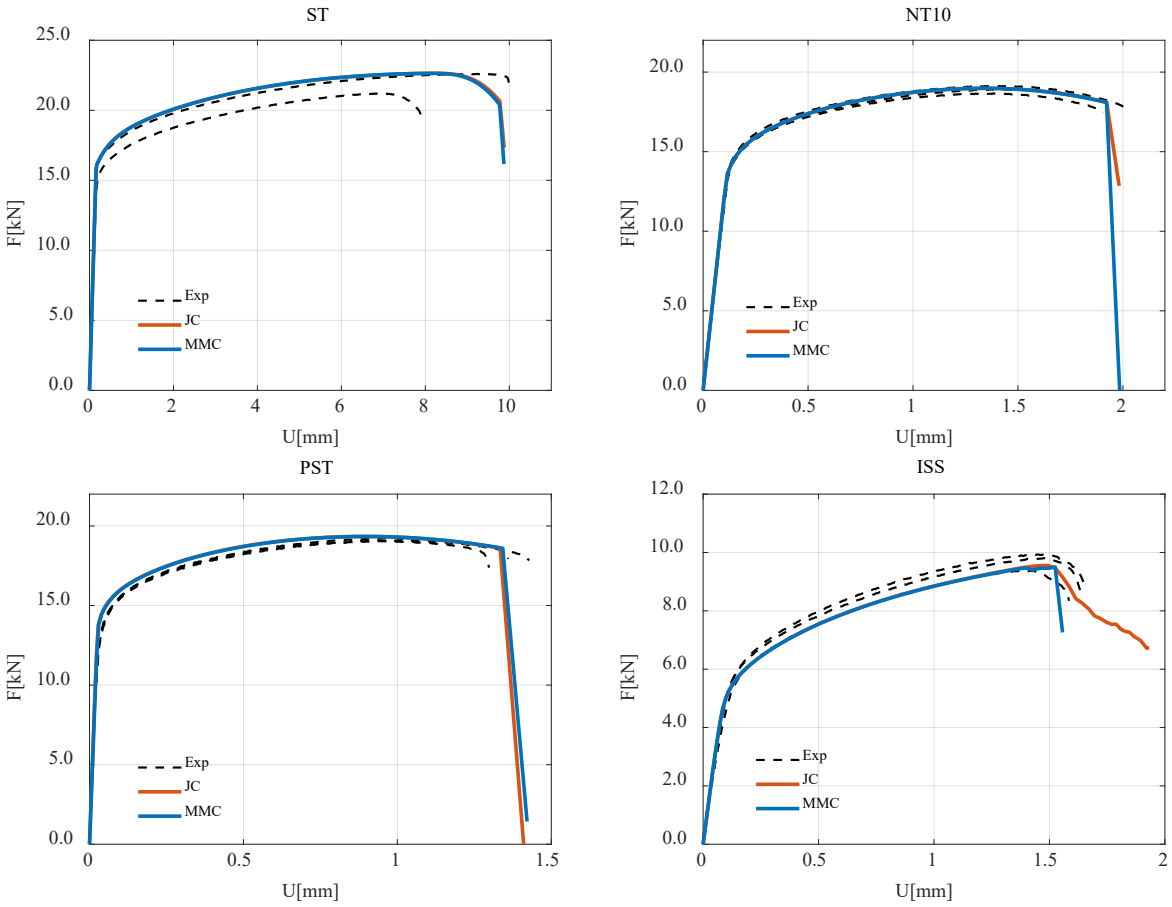

Fig. 3. Experimental comparison of JC and MMC damage models. Force vs. displacement curves for 4 tensile specimens.

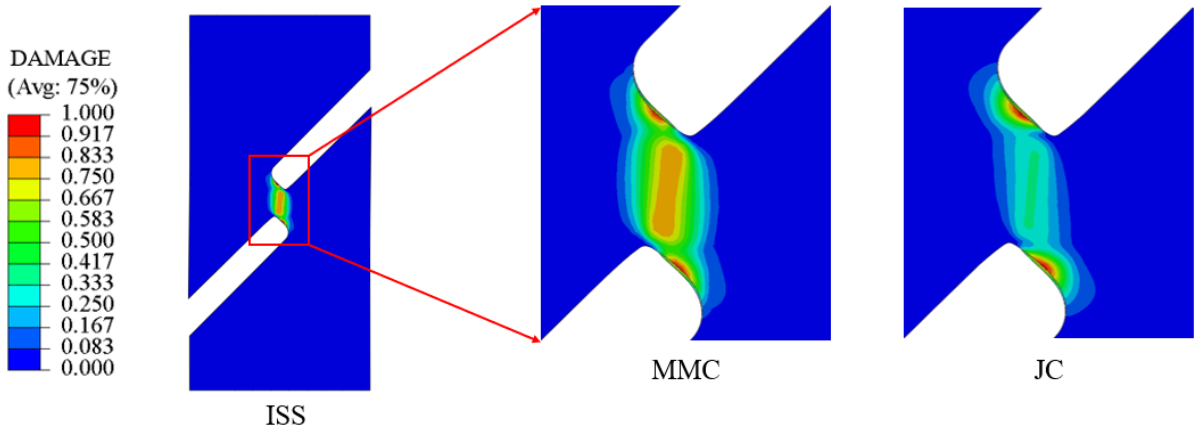

Fig. 4. Comparison JC and MMC damage distribution for ISS at the onset of failure.

In Fig. 4, the damage distributions at the onset of failure are plotted for the ISS specimen using the JC and MMC models. The JC model is known to be insufficient at predicting failure in shear dominant loads due to the lack of Lode parameter effect. One can see that in the gauge section, the JC model predicts lower damage values compared to the MMC model. This results in a gradual decrease of load for the JC model while the MMC model yields a sudden drop after the initiation of failure which is more compatible with the experimental observations.

Materials Research Proceedings 28 (2023) 807-816 https://doi.org/10.21741/9781644902479-88

Flow Forming Process Simulations.

The verified damage models are applied for the simulation of the flow forming process with two different preform geometries. Geometries differ by their thickness to inner diameter ratios. Preform 2 has double thickness to diameter ratio compared to Preform 1. Simulations are performed at the same feed rate, revolution speed, and the other geometrical parameters are kept constant. Simulation results are depicted in Fig. 5. The highest damage is predicted to be at the inner surfaces where the preform is in contact with the mandrel for both models. Due to the shear dominant nature of the process, the JC model gives significantly smaller damage accumulations compared to the MMC model. At 40% reduction, the damage exceeds 1 with the MMC model while it is much less than 1 for the JC model. With a higher thickness to diameter ratio, the damage is found to increase and spread over a larger area. It is normally expected that the crack would form on the outer surface of the flow formed specimen, which is not captured with the current models. However, referring to a previous study of the authors [15], a more realistic modeling approach with temperature dependent plasticity and damage models is important and would change the damage distribution.

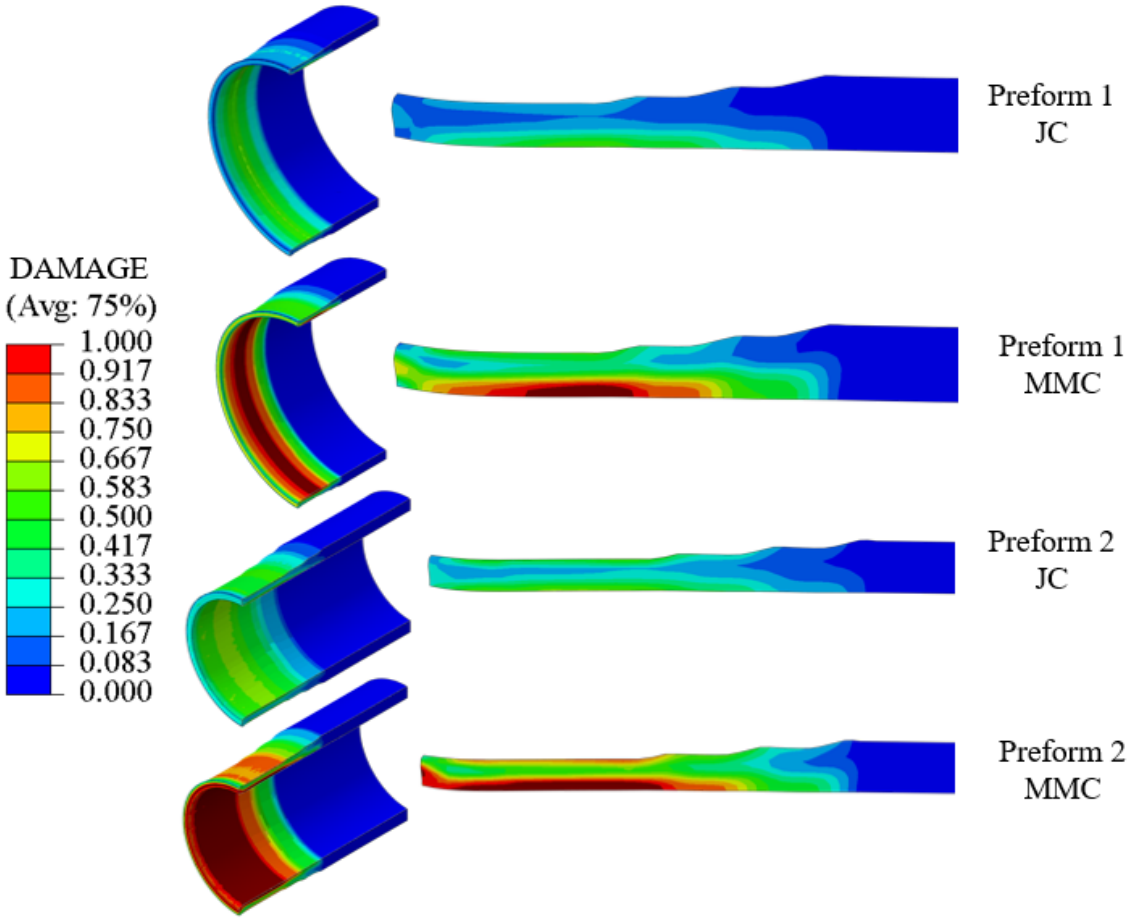

Fig. 5. Distribution of damage over the preform at 2 different geometries.

Summary
In this work, ductile failure model calibration is performed with experiments using four geometries for IN718 nickel alloy. Calibrated models are then verified through FE element analysis of the specimens and results are found to be in good agreement with experimental data. The MMC model is more capable of predicting experimental force-displacement curves in the shear dominant failure case. Furthermore, the two damage models are implemented in a flow forming simulation to discuss the differences in damage accumulation. Models show a disparity in the distribution of damage at two different preform geometries. It is concluded that the MMC failure criterion is a more appropriate choice for forming processes such as flow forming. It should be noted that the current FE model should be extended to include temperature and strain rate effects to accurately make an experimentally comparative study.

References
[1] A. Karakas, T.O. Fenercioğlu, T. Yalçinkaya, The influence of flow forming on the precipitation characteristics of Al2024 alloys, Mater. Lett. 299 (2021) 130066. https://doi.org/10.1016/j.matlet.2021.130066
[2] A.L. Gurson, Continuum theory of ductile rupture by void nucleation and growth: part I—yield criteria and flow rules for porous, J. Eng. Mater. Technol. 99 (1977) 2-15. https://doi.org/10.1115/1.3443401
[3] J. Lemaitre, Coupled elasto-plasticity and damage constitutive equations, Comput. Methods Appl. Mech. Eng. 51 (1985) 31-49. https://doi.org/10.1016/0045-7825(85)90026-X
[4] T. Yalçinkaya, C. Erdogan, I.T. Tandogan, A. Cocks, Formulation and implementation of a new porous plasticity model, Procedia Struct. Integr. 21 (2019) 46-51. https://doi.org/10.1016/j.prostr.2019.12.085
[5] G.R. Johnson, W.H. Cook, Fracture characteristics of three metals subjected to various strains, strain rates, temperatures and pressures, Eng. Fract. Mech. 21 (1985) 31-48. https://doi.org/10.1016/0013-7944(85)90052-9
[6] Y. Bai, T. Wierzbicki, A new model of metal plasticity and fracture with pressure and Lode dependence, Int. J. Plast. 24 (2008) 1071-1096. https://doi.org/10.1016/j.ijplas.2007.09.004
[7] T. Wierzbicki, Y. Bao, Y.W. Lee, Y. Bai, Calibration and evaluation of seven fracture models, Int. J. Mech. Sci. 47 (2005) 719-743. https://doi.org/10.1016/j.ijmecsci.2005.03.003
[8] Y. Bai, T. Wierzbicki, Application of extended mohr-coulomb criterion to ductile fracture. Int. J. Fract., 161 (2010) 1-20. https://doi.org/10.1007/s10704-009-9422-8
[9] D. Mohr, S.J. Marcadet, Micromechanically-motivated phenomenological Hosford-Coulomb model for predicting ductile fracture initiation at low stress triaxialities, Int. J. Solid Struct. 67-68 (2015) 40-55. https://doi.org/10.1016/j.ijsolstr.2015.02.024
[10] R. Li, Z. Zheng, M. Zhan, H. Zhang, Y. Lei, A comparative study of three forms of an uncoupled damage model as fracture judgment for thin-walled metal sheets, Thin-Walled Struct. 169 (2021) 108321. https://doi.org/10.1016/j.tws.2021.108321
[11] W. Xu, H. Wu, H. Ma, D. Shan, Damage evolution and ductile fracture prediction during tube spinning of titanium alloy, Int. J. Mech. Sci. 135 (2018) 226-239. https://doi.org/10.1016/j.ijmecsci.2017.11.024
[12] H. Wu, W. Xu, D. Shan, B.C. Jin, An extended gtn model for low stress triaxiality and application in spinning forming, J. Mater. Process. Technol. 263 (2019) 112-128. https://doi.org/10.1016/j.jmatprotec.2018.07.032
[13] A.K. Singh, A. Kumar, K.L. Narasimhan, R. Singh, Understanding the deformation and fracture mechanisms in backward flow-forming process of Ti-6Al-4V alloy via a shear modified

continuous damage model, J. Mater. Process. Technol. 292 (2021) 117060. https://doi.org/10.1016/j.jmatprotec.2021.117060
[14] H. Vural, C. Erdoğan, T.O. Fenercioğlu, T. Yalçinkaya, Ductile failure prediction during the flow forming process, Procedia Struct. Integr. 35 (2022) 25-33. https://doi.org/10.1016/j.prostr.2021.12.044
[15] C. Erdogan, H. Vural, T.O. Fenercioglu, T. Yalcinkaya, Effect of process parameters on ductile failure behavior of flow forming process, Procedia Struct. Integr. 42 (2022) 1643-1650. https://doi.org/10.1016/j.prostr.2022.12.207